Mon. Not. R. Astron. Soc. **377,** 1747–1762 (2007) doi:10.1111/j.1365-2966.2007.11743.x

SW Sextantis stars: the dominant population of cataclysmic variables with orbital periods between 3 and 4 h

P. Rodríguez-Gil,[1,2⋆] B. T. Gänsicke,[2] H.-J. Hagen,[3] S. Araujo-Betancor,[1] A. Aungwerojwit,[2,4] C. Allende Prieto,[5] D. Boyd,[6] J. Casares,[1] D. Engels,[3] O. Giannakis,[7] E. T. Harlaftis,[8] J. Kube,[9] H. Lehto,[10,11] I. G. Martínez-Pais,[1,12] R. Schwarz,[13] W. Skidmore,[14] A. Staude[13] and M. A. P. Torres[15]

[1]*Instituto de Astrofísica de Canarias, Vía Láctea s/n, La Laguna, E-38205 Santa Cruz de Tenerife, Spain*
[2]*Department of Physics, University of Warwick, Coventry CV4 7AL*
[3]*Hamburger Sternwarte, Universität Hamburg, Gojenbergsweg 112, 21029 Hamburg, Germany*
[4]*Department of Physics, Faculty of Science, Naresuan University, Phitsanulok 65000, Thailand*
[5]*McDonald Observatory and Department of Astronomy, University of Texas, Austin, TX 78712, USA*
[6]*British Astronomical Association, Variable Star Section, West Challow OX12 9TX*
[7]*Institute of Astronomy and Astrophysics, National Observatory of Athens, PO Box 20048, Athens 11810, Greece*
[8]*Institute of Space Applications and Remote Sensing, National Observatory of Athens, PO Box 20048, Athens 11810, Greece*
[9]*Alfred-Wegener-Institut für Polar- und Meeresforschung, Bürgermeister-Smidt-Straße 20, 27568 Bremerhaven, Germany*
[10]*Tuorla Observatory, University of Turku, FIN-21500 Piikkiö, Finland*
[11]*Department of Physics, FIN-20014 University of Turku, Finland*
[12]*Departamento de Astrofísica, Universidad de La Laguna, Tenerife, Spain*
[13]*Astrophysikalisches Institut Potsdam, An der Sternwarte 16, 14482 Potsdam, Germany*
[14]*California Institute of Technology, Mail Code 105-24, Pasadena, CA 91125-24, USA*
[15]*Harvard–Smithsonian Center for Astrophysics, 60 Garden Street, Cambridge, MA 02138, USA*

Accepted 2007 March 15. Received 2007 March 8; in original form 2007 February 9

ABSTRACT

We present time-series optical photometry of five new cataclysmic variables (CVs) identified by the Hamburg Quasar Survey (HQS). The deep eclipses observed in HS 0129+2933 (= TT Tri), HS 0220+0603 and HS 0455+8315 provided very accurate orbital periods of 3.35129827(65), 3.58098501(34) and 3.56937674(26) h, respectively. HS 0805+3822 shows grazing eclipses and has a likely orbital period of 3.2169(2) h. Time-resolved optical spectroscopy of the new CVs (with the exception of HS 0805+3822) is also presented. Radial velocity studies of the Balmer emission lines provided an orbital period of 3.55 h for HS 1813+6122, which allowed us to identify the observed photometric signal at 3.39 h as a negative superhump wave. The spectroscopic behaviour exhibited by all the systems clearly identifies them as new SW Sextantis (SW Sex) stars. HS 0220+0603 shows unusual N II and Si II emission lines suggesting that the donor star may have experienced nuclear evolution via the CNO cycle.

These five new additions to the class increase the number of known SW Sex stars to 35. Almost 40 per cent of the total SW Sex population do not show eclipses, invalidating the requirement of eclipses as a defining characteristic of the class and the models based on a high orbital inclination geometry alone. On the other hand, as more SW Sex stars are identified, the predominance of orbital periods in the narrow 3–4.5 h range is becoming more pronounced. In fact, almost *half* the CVs which populate the 3–4.5 h period interval are definite members of the class. The dominance of SW Sex stars is even stronger in the 2–3 h period gap, where they make up 55 per cent of all known gap CVs. These statistics are confirmed by our results from the HQS CVs. Remarkably, 54 per cent of the Hamburg nova-like variables have been

⋆E-mail: prguez@iac.es

identified as SW Sex stars with orbital periods in the 3–4.5 h range. The observation of this pile-up of systems close to the upper boundary of the period gap is difficult to reconcile with the standard theory of CV evolution, as the SW Sex stars are believed to have the highest mass-transfer rates among CVs.

Finally, we review the full range of common properties that the SW Sex stars exhibit. Only a comprehensive study of this rich phenomenology will prompt to a full understanding of the phenomenon and its impact on the evolution of CVs and the accretion processes in compact binaries in general.

Key words: accretion, accretion discs – binaries: close – novae, cataclysmic variables.

1 INTRODUCTION

The Palomar–Green survey (Green, Schmidt & Liebert 1986) led to the identification of several relatively bright ($V \sim 15$), deeply eclipsing cataclysmic variables (CVs) with orbital periods in the range 3–4 h, namely SW Sex (Penning et al. 1984), DW UMa (Shafter, Hessman & Zhang 1988), BH Lyn (Thorstensen, Davis & Ringwald 1991a; Dhillon et al. 1992) and PX And (Thorstensen et al. 1991b). Szkody & Piché (1990) and Thorstensen et al. (1991b) established a number of common traits among these systems, including unusually 'V'-shaped eclipse profiles, the presence of He II λ4686 emission, a substantial orbital phase lag (∼0.2 cycle) of the radial velocities of the Balmer lines with respect to the motion of the white dwarf, and single-peaked emission lines that display central absorption dips around orbital phases ≃0.4–0.7. The 'SW Sextantis (SW Sex) phenomenon' was later extended to lower orbital inclinations after the identification of several grazingly eclipsing and non-eclipsing CVs which exhibit the spectroscopic properties characteristic of the SW Sex class (WX Ari: Beuermann et al. 1992; Rodríguez-Gil et al. 2000; V795 Her: Casares et al. 1996; LS Peg: Martínez-Pais, Rodríguez-Gil & Casares 1999; Taylor, Thorstensen & Patterson 1999; V442 Oph: Hoard, Thorstensen & Szkody 2000).

The observational characteristics of the SW Sex stars are not easily reconciled with the properties of a simple, steady-state hot optically thick accretion disc which is expected to be found in intrinsically bright, weakly-magnetic CVs above the period gap. Nevertheless, a variety of mechanisms have been invoked to explain the behaviour of the SW Sex stars, such as stream overflow (Hellier & Robinson 1994; Hellier 1996), magnetic white dwarfs (Williams 1989; Casares et al. 1996; Rodríguez-Gil et al. 2001; Hameury & Lasota 2002), magnetic propellers in the inner disc (Horne 1999), and self-obscuration of the inner disc (Knigge et al. 2000). While no unambiguous model for their accretion geometry has been found so far, it is becoming increasingly clear that the SW Sex stars are not rare and unusual systems, but represent an important, if not dominant fraction of all CVs in the orbital period range 3–4 h (Aungwerojwit et al. 2005; Rodríguez-Gil 2005). Hence, a thorough investigation of this class of systems is important in the context of understanding CV evolution as a whole.

In this paper, we present five new CVs identified in the Hamburg Quasar Survey (HQS; Hagen et al. 1995) which are classified as new SW Sex stars on the basis of our follow-up photometry and spectroscopy. The new discoveries bring the total number of confirmed SW Sex stars to 35, and we discuss the global properties of these objects as a class.

2 OBSERVATIONS AND DATA REDUCTION

2.1 Identification

The five new CVs (Fig. 1) were selected for follow-up observations upon the detection of emission lines in their HQS spectra. Identification spectra of HS 0220+0603, HS 0805+3822 and HS 1813+6122 were, respectively, obtained in 1990 October with the Calar Alto 3.5-m telescope, in 1996 December with the 1.5-m Tillinghast telescope at Fred Lawrence Whipple Observatory, and in 1991 June with the Calar Alto 2.2-m telescope as part of quasi-stellar object and galaxy searches. HS 0129+2933 and HS 0455+8315 were both identified as CVs in 2000 September using the Calar Alto 2.2-m telescope as part of a dedicated search for CVs in the HQS (Gänsicke, Hagen & Engels 2002).

HS 0129+2933 (= TT Tri) was already identified as an eclipsing star by Romano (1978). At the time of writing this paper we were aware of a multicolour photometric study by Warren, Shafter & Reed (2006), in which an eclipse ephemeris is derived for the first time.

HS 0805+3822 was independently found as a CV in the Sloan Digital Sky Survey (SDSS J080908.39+381406.2, Szkody et al. 2003) and was identified as an SW Sex star.

Flux-calibrated, low-resolution identification spectra of the five new CVs are shown in Fig. 2. The spectra are dominated by strong, single-peaked Balmer and He I emission lines on top of blue continua. The high-excitation emission lines of He II λ4686 and the C III/N III Bowen blend near 4640 Å are also observed, and are especially intense in HS 0455+8315. Table 1 summarizes some properties of the new CVs.

2.2 Optical photometry

We obtained differential CCD photometry of the five new CVs at seven different telescopes: the 2.2-m telescope at Calar Alto Observatory, the 1.2-m telescope at Kryoneri Observatory, the 0.82-m IAC80 and the 1-m Optical Ground Station at Observatorio del Teide, the 0.7-m telescope of the Astrophysikalisches Institut Potsdam, the 1.2-m telescope at Fred Lawrence Whipple Observatory, and the 0.7-m Schmidt-Väisälä telescope at Tuorla Observatory, and the 0.35-m telescope at West Challow Observatory. Details on the instrumentation are given in the notes to Table 3, which also contains the log of the photometric observations. The data obtained at Calar Alto, Kryoneri and Tuorla were reduced with the pipeline described by Gänsicke et al. (2004), which applies bias and flat-field corrections in MIDAS and then uses SEXTRACTOR (Bertin

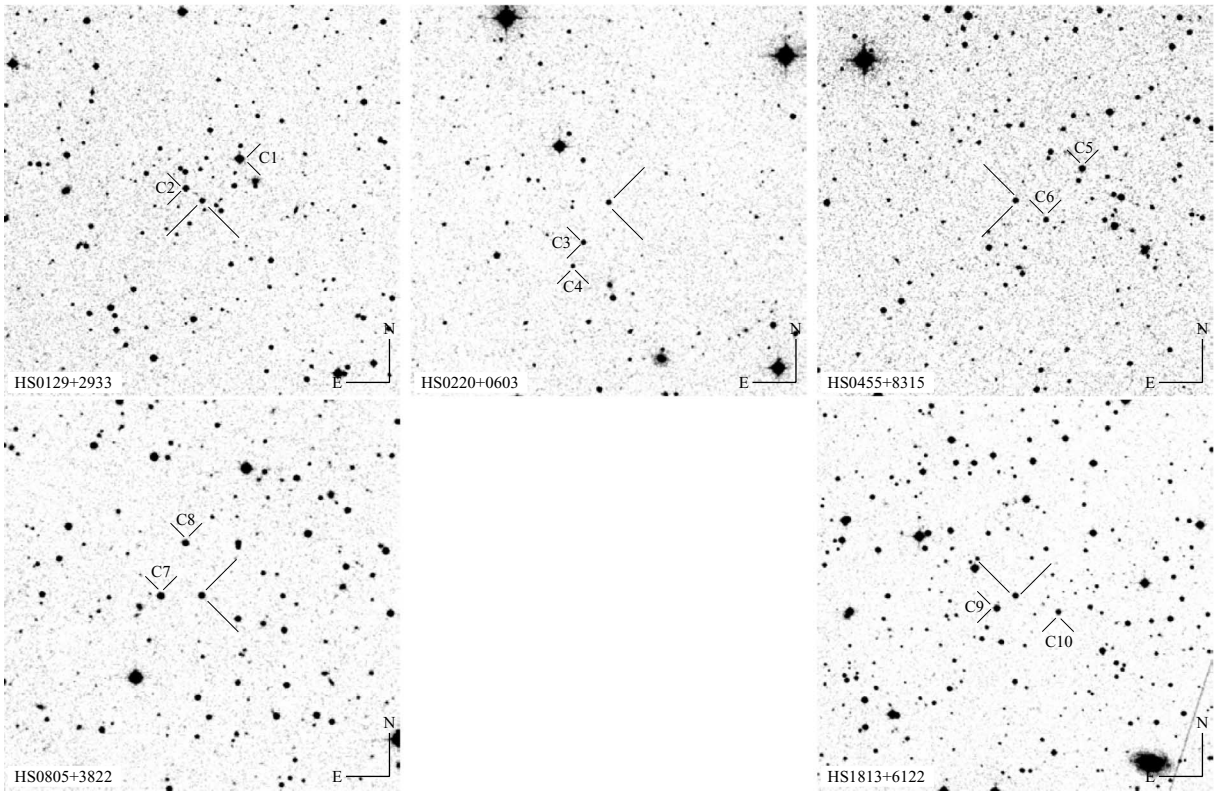

Figure 1. 10×10-arcmin^2 finding charts for HS 0129+2933, HS 0220+0603, HS 0455+8315, HS 0805+3822 and HS 1813+6122 obtained from the Digitized Sky Survey. See Table 2 for details on the comparison stars C1–C10.

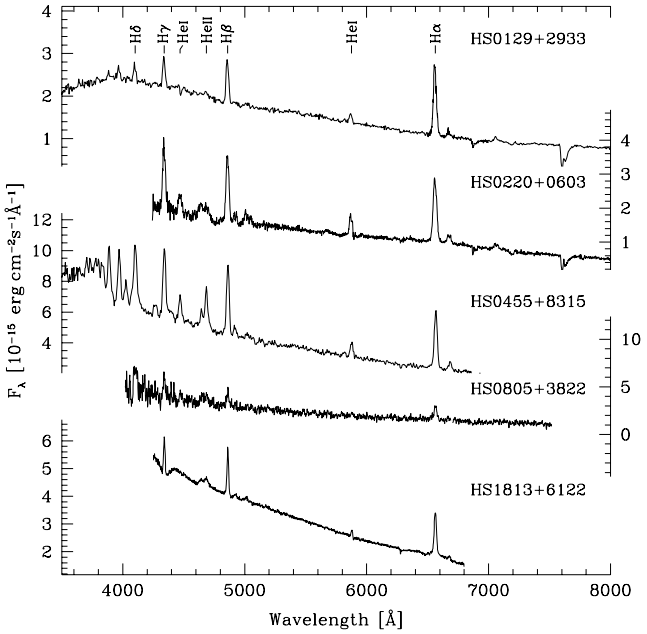

Figure 2. Flux-calibrated optical spectra of the five new CVs.

& Arnouts 1996) to extract aperture photometry for all objects in the field of view. The reduction of the Astrophysikalisches Institut Potsdam data was carried out completely using MIDAS. IRAF[1] was used to correct the OGS, IAC80 and FLWO data for the bias level and flat-field variations, and to compute point spread function magnitudes of the target and comparison stars. Fig. 1 shows finding charts for the five new CVs and indicates the comparison stars used for differential photometry. The USNO *R* and *B* magnitudes of the comparison stars are given in Table 2. Sample light curves are shown in Fig. 4. HS 0129+2933, HS 0220+0603 and HS 0455+8315 are deeply eclipsing, HS 0805+3822 displays evidence for grazing eclipses (similar to WX Ari, Rodríguez-Gil et al. 2000), and all five systems show substantial short time-scale variability. From the scatter in the comparison star light curves we estimate that the differential photometry is accurate to 1 per cent.

[1] IRAF is distributed by the National Optical Astronomy Observatories.

2.3 Optical spectroscopy

The spectroscopic data were obtained with five different telescopes: the 2.5-m Isaac Newton Telescope (INT) and the 2.56-m Nordic Optical Telescope (NOT) on La Palma, the 2.2-m and the 3.5-m telescopes at Calar Alto Observatory, and the 2.7-m telescope at McDonald Observatory. The log of spectroscopic observations can also be found in Table 3. Details on the different telescope/spectrograph set-ups are given as follows.

(i) At the INT we used the Intermediate Dispersion Spectrograph (IDS) with the R632V grating, the 2048×4100 pixel EEV10a CCD detector, and a 1.1 arcsec slit width. With this set-up we sampled the wavelength region λλ4400–6700 at a resolution (full width at half-maximum, hereafter FWHM) of ∼2.5 Å.

(ii) The Andalucía Faint Object Spectrograph and Camera (ALFOSC) was in place at the NOT. The spectra were imaged on the 2048×2048 pixel EEV chip (CCD #8). A spectral resolution

Table 1. Properties of the five new SW Sex stars. The coordinates and the *B* and *R* magnitudes were taken from the USNO-B catalogue (Monet et al. 2003). The *J*, *H* and K_s magnitudes were taken from the Two-Micron All-Sky Survey (2MASS) catalogue. The emission-line parameters are measured from the public SDSS spectrum.

	HS 0129+2933	HS 0220+0603	HS 0455+8315	HS 0805+3822	HS 1813+6122
Right ascension (J2000)	$01^h31^m59.86^s$	$02^h23^m01.65^s$	$05^h06^m48.27^s$	$08^h09^m08.40^s$	$18^h14^m29.83^s$
Declination (J2000)	$+29^\circ49'22.3''$	$+06^\circ16'50.0''$	$+83^\circ19'23.3''$	$+38^\circ14'06.5''$	$+61^\circ23'34.5''$
Orbital period (h)	3.35129827(65)	3.58098501(34)	3.56937674(26)	$\simeq 3.22$	$\simeq 3.38$
B/*R* magnitudes	15.3/14.7	16.5/16.2	15.2/14.6	14.7/14.6	15.1/14.5
$J/H/K_s$ magnitudes	14.6/14.4/14.3	15.4/15.1/14.8	14.4/14.3/14.1	15.3/15.2/14.9	14.8/14.7/14.6
Hα EW [Å]/FHWM [km s^{-1}]	61/1160	73/1390	50/1180	25/1040	22/1050
Hβ EW [Å]/FHWM [km s^{-1}]	25/1265	43/1560	29/1250	11/970	6/1020
Hγ EW [Å]/FHWM [km s^{-1}]	16/1350	25/1545	31/1540	10/1010	5/930
He I λ5876 EW [Å]/FHWM [km s^{-1}]	8/1120	15/1270	–/–	2/720	1/720
He I λ6678 EW [Å]/FHWM [km s^{-1}]	5/1090	9/1240	10/1240	4/830	–/–
He II λ4686 EW [Å]/FHWM [km s^{-1}]	–/–	6/2190	17/1900	4/700	–/–

Table 2. Comparison stars used for the differential CCD photometry (see Fig. 1).

ID	USNO-A2.0	*R*	*B*
C01	1125-00509642	13.3	14.0
C02	1125-00510117	14.8	15.2
C03	0900-00553937	15.8	17.7
C04	0900-00554015	16.4	18.9
C05	1725-00217755	13.8	15.1
C06	1725-00218117	15.4	15.9
C07	1275-07186372	15.0	15.0
C08	1275-07186091	15.7	17.2
C09	1500-06459684	14.6	15.1
C10	1500-06458763	15.8	16.5

of ∼3.7 Å (FHWM) was achieved by using the grism #7 (plus the second-order blocking filter WG345) and a 1 arcsec slit width. The useful wavelength interval this configuration provides is $\lambda\lambda$3800–6800.

(iii) The spectroscopy at the 2.2-m Calar Alto telescope was performed with CAFOS. A 1.2 arcsec slit width and the G-100 grism granted access to the $\lambda\lambda$4200–8300 range with a resolution of ∼4.5 Å (FWHM) on the standard SITe CCD (2048 × 2048 pixel).

(iv) The double-armed TWIN spectrograph was used to carry out the observations at the 3.5-m telescope in Calar Alto. The blue arm was equipped with the T05 grating, while the T06 grating was in place in the red arm. The wavelength ranges $\lambda\lambda$4070–5160 and $\lambda\lambda$6080–7180 were sampled at 1.32- and 1.23-Å resolution (FWHM; 1.5 arcsec slit width) in the blue and red, respectively.

(v) The Large Cassegrain Spectrometer (LCS) on the 2.7-m telescope at McDonald Observatory was equipped with grating #43 and the TI1 800 × 800 pixel CCD detector. The use of a 1.0 arcsec slit width resulted in a resolution of 3 Å (FWHM) and a wavelength range of $\lambda\lambda$3800–5030.

After the effects of bias and flat-field structure were removed from the raw images, the sky background was subtracted. The one-dimensional target spectra were then obtained using the optimal extraction algorithm of Horne (1986). For wavelength calibration, a low-order polynomial was fitted to the arc data, the *rms* being always smaller than one-tenth of the dispersion in all cases. The pixel-wavelength correspondence for each target spectrum was obtained by interpolating between the two nearest arc spectra. These reduction steps were performed with the standard packages for long-slit spectra within IRAF.

2.4 *HST*/STIS far-ultraviolet spectroscopy

A single far-ultraviolet (FUV) spectrum of HS 0455+8315 was obtained with the *Hubble Space Telescope*/Space Telescope Imaging Spectrograph (*HST*/STIS) as part of a large survey of the FUV emission of CVs (Gänsicke et al. 2003). The data were obtained using the G140L grating and the 5×0.2 − arcsec^2 aperture, resulting in a spectral resolution of $\lambda/\Delta\lambda \simeq 1000$ and a wavelength coverage of $\lambda\lambda$1150–1710. The spectrum was obtained at an orbital phase of $\simeq 0.75$, well outside the eclipse (see Section 4.5). The STIS acquisition image showed the system at an approximate R_c magnitude of 15.4, close to the normal high-state brightness.

3 PHOTOMETRIC PERIODS

3.1 HS 0129+2933, HS 0220+0603 and HS 0455+8315

The deep eclipses detected in the light curves of HS 0129+2933, HS 0220+0603 and HS 0455+8315 provide accurate information on the orbital periods of the systems. Determining the time of mid-eclipse[2] in SW Sex stars is notoriously difficult due to the asymmetric shape of the eclipse profiles. We have therefore employed the following method. The observed eclipse profile is mirrored in time around an estimate of the eclipse centre, and the mirrored profile is overplotted on the original eclipse data. The time of mid-eclipse is then varied until the central part of both eclipse profiles overlaps as closely as possible. This empirical method proved to be somewhat more robust compared to, for example, fitting a parabola to the eclipse profile. The mid-eclipse times are reported in Table 4. An initial estimate of the cycle count was then obtained by fitting eclipse phases $(\phi_0^{\rm observed} - \phi_0^{\rm fit})^{-2}$ over a wide range of trial periods (Fig. 3). Once an unambiguous cycle count was established, a linear eclipse ephemeris was fitted to the times of mid-eclipse. For HS 0129+2933, we also included the 22 eclipse timings reported by Warren et al. (2006) in our calculations. The resulting ephemerides are

$$T_0({\rm HJD}) = 245\,2540.532\,44(21) + 0.139\,637\,428(27)\,E \qquad (1)$$

for HS 0129+2933, that is, $P_{\rm orb} = 3.351\,298\,27(65)$ h,

[2] The time of mid-eclipse, T_0, is the time of inferior conjunction of the donor star.

Table 3. Log of the observations.

Date	UT	Telescope	Filter/Grism	Exposure time (s)	Frames
HS 0129+2933					
2002 August 29	03:22-04:35	INT	*R632V*	600	7
2002 August 31	05:00-05:40	INT	*R632V*	600	4
2002 September 2	04:20-05:01	INT	*R632V*	600	4
2002 September 3	04:39-05:20	INT	*R632V*	600	4
2003 December 17	19:33-01:11	NOT	Grism #7	600	27
2002 September 22	23:42-03:35	KY	*R*	10	1035
2003 September 29	05:29-06:00	IAC80	Clear	15	75
2003 December 15	18:24-23:56	CA22	Clear	15	641
2003 December 16	18:07-19:35	CA22	Clear	20	151
2003 December 25	20:06-21:52	CA22	Clear	15	176
2006 November 21	22:22-23:39	WCO	Clear	60	73
2006 December 11	18:49-19:11	WCO	Clear	60	22
2006 December 16	22:21-23:38	WCO	Clear	60	73
HS 0220+0603					
2002 October 15	23:13-02:47	KY	*R*	25	328
2002 October 17	01:13-03:44	KY	*R*	25	279
2002 December 8	23:27-00:13	CA22	*G-200*	600	4
2002 December 16	18:25-19:20	CA22	*G-200*	600	5
2002 December 29	20:39-23:41	CA22	*V*	30	217
2002 December 31	18:30-21:02	CA22	*V*	30	145
2003 January 26	19:41-23:01	IAC80	*V*, *R*	100	119
2003 January 28	19:24-23:24	IAC80	*V*	120	102
2003 July 11	04:19-05:10	OGS	Clear	50	54
2003 July 13	04:08-05:25	OGS	Clear	30	119
2003 September 22	03:07-04:16	IAC80	Clear	30	100
2003 September 29	00:07-01:24	IAC80	Clear	30	113
2003 November 9	00:50-02:03	IAC80	*R*	60	58
2003 November 17	23:41-00:27	OGS	Clear	17	108
2003 December 15	19:28-21:04	NOT	Grism #7	600	9
2003 December 16	19:26-02:33	NOT	Grism #7	600	38
2006 November 21	19:15-20:11	WCO	Clear	60	55
2006 December 11	19:16-19:49	WCO	Clear	60	33
2006 December 11	22:47-23:23	WCO	Clear	60	36
2006 December 16	21:04-22:16	WCO	Clear	60	70
HS 0455+8315					
2000 October 20	18:57-21:44	AIP	*R*	60	142
2000 November 10	17:30-21:48	AIP	*R*	30	364
2000 November 16	16:45-21:14	AIP	*R*	30	425
2000 December 4	17:09-17:50	AIP	*R*, *B*	30	64
2000 December 5	16:39-18:03	AIP	*R*, *B*	30	135
2000 January 1	03:30-05:31	CA35	*T05/T06*	600	11
2001 January 1	23:03-23:45	CA35	*T05/T06*	300	5
2001 January 2	00:32-04:38	CA35	*T05/T06*	400	33
2002 December 9	09:06	*HST*	*G140L*	730	1
2006 November 21	20:30-22:02	WCO	Clear	60	88
2006 November 23	23:05-00:09	WCO	Clear	60	62
2006 December 8	20:05-21:03	WCO	Clear	50	68
2007 January 11	21:28-22:40	WCO	Clear	60	70
2007 January 13	23:33-00:15	WCO	Clear	50	50
2007 January 14	21:01-21:52	WCO	Clear	50	60
HS0805+3822					
2005 February 11	19:28-04:32	Tuorla	Clear	90	325
2005 February 15	18:36-01:03	Tuorla	Clear	80	257
2005 February 28	04:39-10:00	FLWO1.2	Clear	15–20	769
2005 March 1	03:12-09:56	FLWO1.2	Clear	15	784
2005 March 4	05:59-09:33	FLWO1.2	Clear	15–25	402
2005 March 24	20:03-00:04	Tuorla	Clear	30	373

Table 3 – *continued*

Date	UT	Telescope	Filter/Grism	Exposure time (s)	Frames
2005 March 25	20:00-02:21	Tuorla	Clear	30	608
2005 March 27	03:07-08:18	FLWO1.2	Clear	15–20	674
2005 March 28	04:06-07:12	FLWO1.2	Clear	15–20	390
2005 March 29	04:48-08:04	FLWO1.2	Clear	15–30	321
HS1813+6122					
2000 September 24	20:23-20:54	CA22	*R-100*	600	2
2001 August 23	21:46-01:26	AIP	*R*	30	346
2001 August 23	20:10-01:05	AIP	*R*	60	251
2001 August 23	19:58-00:20	AIP	*R*	60	199
2002 July 3	23:47-02:29	KY	*R*	120	67
2002 July 5	19:54-22:31	KY	*R*	120	69
2002 August 22	18:44-21:36	KY	Clear	10	660
2002 August 23	18:59-22:21	KY	Clear	10	800
2002 September 4	21:24-23:58	KY	*R*	10	516
2002 September 4	00:23-00:54	INT	*R632V*	600	4
2002 September 6	18:34-21:57	KY	*R*	35	276
2003 August 20	18:11-21:43	KY	Clear	10	649
2002 August 27	22:38-00:11	INT	*R632V*	600	9
2002 August 31	23:37-00:28	INT	*R632V*	600	5
2002 September 1	21:55-22:37	INT	*R632V*	600	4
2002 September 3	20:26-21:07	INT	*R632V*	600	4
2003 June 28	22:49-00:35	KY	*R*	60	93
2003 July 15	02:29-05:09	OGS	Clear	15	442
2003 September 23	20:23-00:05	IAC80	Clear	7	690
2003 September 24	20:02-22:50	IAC80	Clear	7	502
2003 September 25	21:18-23:48	IAC80	Clear	10	400
2003 September 26	19:53-21:08	IAC80	Clear	7	248
2003 September 27	19:36-23:19	IAC80	Clear	7	680
2003 May 18	01:00-04:08	INT	*R632V*	600	6
2003 May 19	02:48-04:13	INT	*R632V*	600	8
2004 May 24	02:13-03:36	IAC80	Clear	15	134
2004 May 25	01:44-05:19	IAC80	Clear	15	411
2004 May 26	00:34-05:15	IAC80	Clear	15	720
2003 June 29	00:52-03:58	CA22	*G-100*	600	15
2003 June 30	03:13-04:11	CA22	*G-100*	600	5
2004 July 17	04:17-04:50	McD	#43	600	3
2004 July 18	04:11-05:19	McD	#43	600	6

Notes on the instrumentation used for CCD photometry. CA22: 2.2-m telescope at Calar Alto Observatory, using CAFOS with a 2 k × 2 k pixel SITe CCD; KY: 1.2-m telescope at Kryoneri Observatory, using a Photometrics SI-502 516 × 516 pixel CCD camera; IAC80: 0.82-m telescope at Observatorio del Teide, equipped with Thomson 1 k × 1 k pixel CCD camera; OGS: 1-m Optical Ground Station at Observatorio del Teide, equipped with Thomson 1 k × 1 k pixel CCD camera; AIP: 0.7-m telescope of the Astrophysikalisches Institut Potsdam, with 1 k × 1 k pixel SITe CCD; FLWO: 1.2-m telescope at Fred Lawrence Whipple Observatory, equipped with MINICAM containing three 2048 × 4608 EEV CCDs; Tuorla: 0.7-m Schmidt-Väisälätelescope at Tuorla Observatory, equipped with a SBIG ST–8 CCD camera; WCO: 0.35-m telescope at West Challow Observatory with SXV-H9 CCD camera.

$$T_0(\mathrm{HJD}) = 245\,2563.574\,036(73) + 0.149\,207\,709(14)\,E \quad (2)$$

for HS 0220+0603, that is, $P_{\mathrm{orb}} = 3.580\,985\,01(34)$ h, and

$$T_0(\mathrm{HJD}) = 245\,1859.244\,63(12) + 0.148\,724\,030(11)\,E \quad (3)$$

for HS 0455+8315, that is, $P_{\mathrm{orb}} = 3.569\,376\,74(26)$ h.

3.2 HS 0805+3822

Some of the light curves of HS 0805+3822 contain broad dips that we interpret as grazing eclipses, similar to those detected in WX Ari (Rodríguez-Gil et al. 2000). The system displays a varying level of short time-scale variability, and we restrict the identification of the (presumed) eclipses to the nights with low flickering activity (Fig. 4, Table 4). No unique cycle count can be determined from the four eclipses detected (Fig. 3), and the eclipse ephemerides determined for the two most likely cycle count aliases are

$$T_0(\mathrm{HJD}) = 245\,3413.4264(22) + 0.126\,7611(75)\,E \quad (4)$$

that is, $P_{\mathrm{orb}} = 3.0423(2)$ h and

$$T_0(\mathrm{HJD}) = 245\,3413.4264(23) + 0.134\,0385(84)\,E \quad (5)$$

that is, $P_{\mathrm{orb}} = 3.2169(2)$ h.

Table 4. Eclipse timings (given in HJD − 245 0000), cycle number, and the difference between observed and computed eclipse times using the ephemerides in equations (1)–(4). See Warren et al. (2006) for additional eclipse timings of HS 0129+2933.

T_0	Cycle	O−C (s)	T_0	Cycle	O−C (s)
HS 0129+2933			2961.51100	2667	−1
2540.532 10	0	−30	4061.321 13	10 038	10
2989.327 39	3214	22	4081.314 81	10 172	−4
2989.467 02	3215	21	4081.463 97	10 173	−8
2990.304 18	3221	−36	4086.387 89	10 206	−2
2999.381 61	3286	50	**HS 0455+8315**		
4061.463 37	10 892	5	1859.246 83	0	−7
4081.292 06	11 034	20	1859.395 49	1	−13
4086.458 40	11 071	−1	1865.344 49	41	−12
HS 0220+0603			1884.23301	168	8
2563.574 52	0	42	1884.233 33	168	24
2564.618 52	7	2	4061.401 38	14 807	−28
2638.476 10	502	−18	4063.483 39	14 821	−13
2666.378 11	689	−3	4078.356 39	14 921	43
2666.378 18	689	3	4112.413 40	15 150	−25
2668.317 51	702	−29	4114.495 83	15 164	0
2668.466 82	703	−20	4115.388 43	15 170	22
2831.700 04	1797	−21	**HS 0805+3822**		
2834.684 39	1817	−5	3413.426 28	0	−9
2904.662 98	2286	10	3455.383 12	313	231
2911.526 46	2332	4	3455.513 61	314	−75
2952.559 00	2607	40	3457.791 44	331	−147

The data of the nights during which grazing eclipses were detected folded over both periods are shown in Fig. 5.

As an alternative approach, we have subjected the combined data from all nights to an analysis-of-variance (after subtracting the nightly mean magnitudes) using Schwarzenberg-Czerny's (1996) method, and find the strongest signal at 3.21 h (Fig. 3). Folding all data on that period gives a light curve which broadly resembles the 'eclipse' light curves mentioned above. We conclude that the orbital period of HS 0805+3822 is ≃3.22 h.

3.3 HS 1813+6122

The light curve of HS 1813+6122 is characterized by rapid (10–20 min) oscillations with a typical amplitude of 0.1−0.2 mag, superimposed by modulations with time-scales of hours and amplitudes of ≃0.1 mag. We combined all data after subtracting the nightly means, and calculated a Scargle (1982) periodogram (Fig. 3, bottom panel). Two broad clusters of signals are found at 3.38 and 3.54 h, with the stronger signal at the shorter period. The same double-cluster structure repeats with lower amplitudes at several ±1 cycle d^{-1} aliases. Fig. 6 shows the photometric data folded on either period, after subtracting a sine fit with the respective other period.

Many of the known SW Sex stars display positive and/or negative superhumps in their light curves (e.g. Patterson & Skillman 1994; Rolfe, Haswell & Patterson 2000; Patterson et al. 2002, 2005; Stanishev et al. 2002), and the pattern observed in HS 1813+6122 fits into that picture. On the basis of photometry alone, it is usually not possible to unambiguously identify orbital and superhump periods, but based on the radial velocity study described below in Section 4.3, we suggest that $P_{\rm SH} = 3.38$ h and $P_{\rm orb} = 3.54$ h.

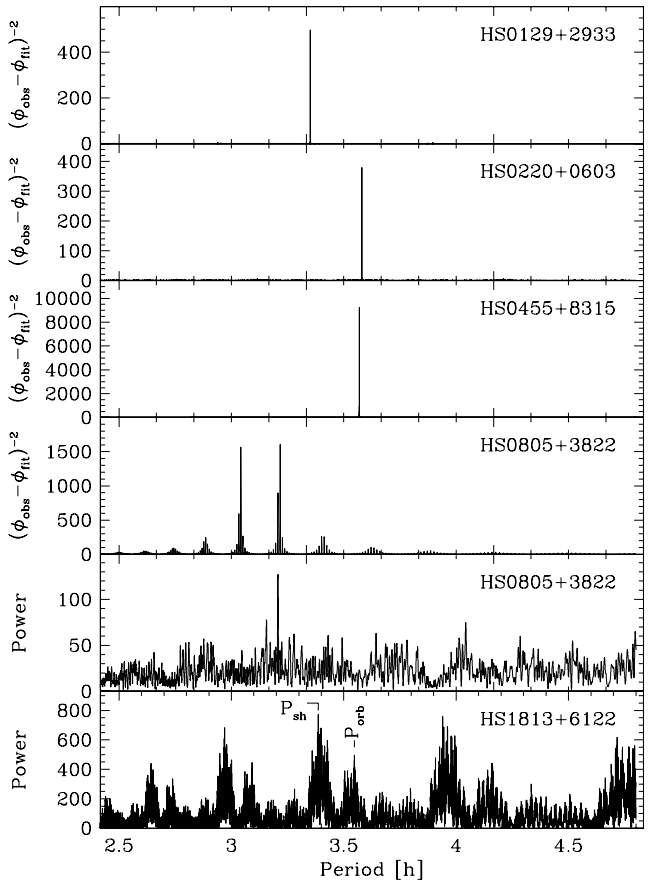

Figure 3. Time-series analysis of the CCD photometry of the five new SW Sex stars. The four top panels show the results of eclipse-phase fits for the deeply eclipsing systems HS 0129+2933, HS 0220+0603 and HS 0455+8315, as well as for the grazing eclipser HS 0805+3822. For HS 0805+3822, an analysis-of-variance periodogram (Schwarzenberg-Czerny 1996) is shown in the second-lowest panel, and a Scargle (1982) periodogram is shown for HS 1813+6122 in the bottom panel, with the likely orbital period and superhump period indicated.

4 SPECTROSCOPIC ANALYSIS

4.1 An overabundance of nitrogen in HS 0220+0603

HS 0220+0603 shows emission lines not usually seen in CVs. In Fig. 7, we plot the average spectrum covering the region λλ4870–6500. We identify a group of lines around λ5250 as Fe II transitions. They very likely are emission profiles plus an absorption component since a deep absorption trough is observed at the position of Fe II λ5169. The He I λ5016 line is abnormally broad and has a strange profile with three peaks. This is probably the effect of blended He I and Fe II emission (at λ5018). However, the most notorious feature is the broad N II λ5680 emission. Another triple-peaked emission-line profile is found at λ6350 which we identify as Si II emission. The N II λ5680 transition has been observed in the intermediate polar HS 0943+1404 (Rodríguez-Gil et al. 2005), and we interpret its presence as evidence of an anomalously large abundance of nitrogen.

An observed overabundance of nitrogen in the accretion flow is directly linked to the chemical abundances of the donor star, and suggests that the donor has undergone nuclear evolution via the CNO cycle. This implies that the donor had an initial mass of $\gtrsim 1.2\,M_\odot$ and the system evolved through a phase of

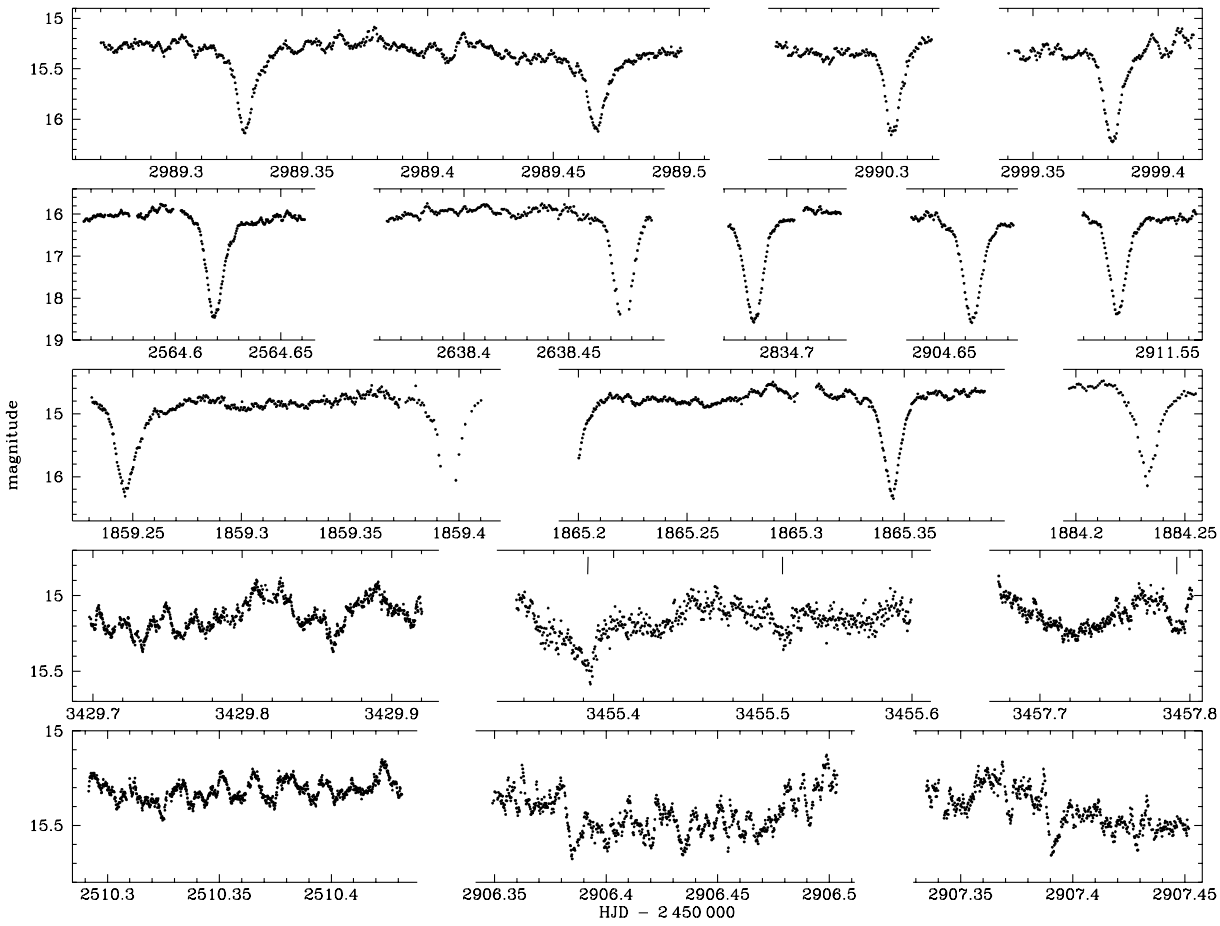

Figure 4. Sample light curves of the five new SW Sex stars. From top to bottom panel: HS 0129+2933, HS 0220+0603, HS 0455+8315, HS 0805+3822 and HS 1813+6122. HS 0805+3822 displays grazing eclipses. Those indicated by the ticks above the light curves were used to calculate an ephemeris.

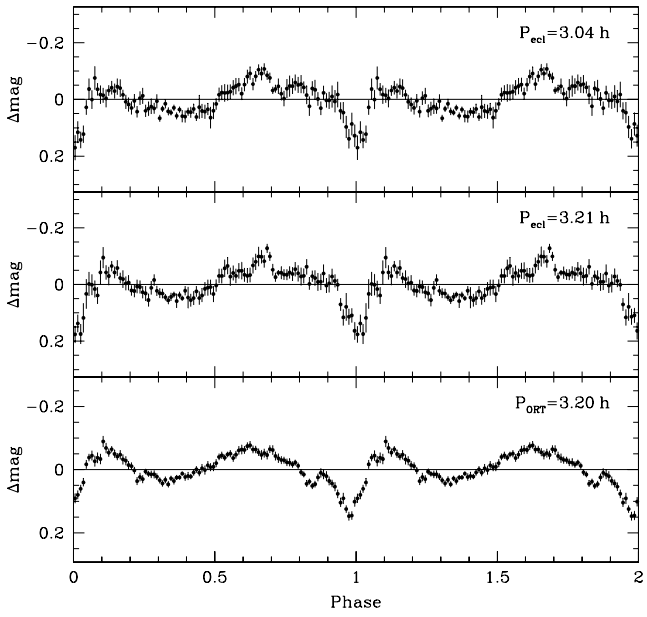

Figure 5. Phase-folded light curves of HS 0805+3822. Top and middle panels: data from the nights with low flickering activity folded over the eclipse ephemerides given by equations (4) and (5). Bottom panel: all data folded over the period determined from an analysis-of-variance periodogram (ORT, Schwarzenberg-Czerny 1996).

thermal-time-scale mass transfer (Schenker et al. 2002; Podsiadlowski, Han & Rappaport 2003). The theoretical models predict that up to one-third of all CVs may have undergone nuclear evolution. This seems to be confirmed by the substantial number of systems with evolved donor stars that have been found (e.g. Jameson, King & Sherrington 1980; Bonnet-Bidaud & Mouchet 1987; Thorstensen et al. 2002a,b; Gänsicke et al. 2003).

4.2 Radial velocities

Radial velocity curves of the Hα and He II λ4686 emission lines were computed for the eclipsing systems, except for HS 0129+2933 where He II λ4686 is too weak and only Hα was measured. The individual velocity points were obtained by cross-correlating the individual profiles with single Gaussian templates matching the FWHMs of the respective average line profiles (see Table 1). Before measuring the velocities, the normalized spectra were re-binned to a uniform velocity scale centred on the rest wavelength of each line. The radial velocity curves of the three deeply eclipsing systems folded on their respective orbital periods are presented in Fig. 8.

We fitted sinusoidal functions of the form

$$V_{\rm r} = \gamma - K \sin\left[2\pi\left(\varphi - \varphi_0\right)\right]$$

to the radial velocity curves. The fitting parameters are shown in Table 5. Note that the γ and K parameters given in the table are

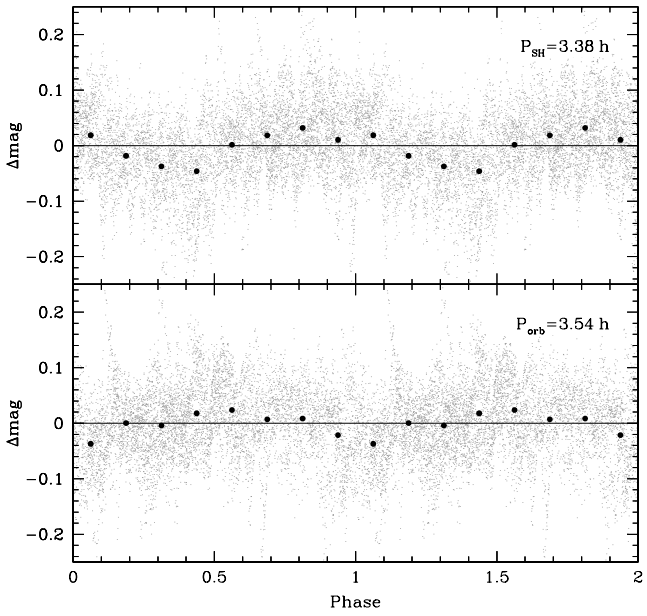

Figure 6. Phase-folded light curves of HS 1813+6122. Top panel: all data folded over $P_{\rm SH} = 3.38$ h, the strongest signal detected in the periodogram (Fig. 3), after subtracting a sine fit with $P_{\rm orb} = 3.54$ h, the period of the neighbouring signal. Bottom panel: all data folded over $P_{\rm orb} = 3.54$ h after subtracting a sine fit with $P_{\rm SH} = 3.38$ h. We interpret $P_{\rm SH}$ and $P_{\rm orb}$ as the superhump and orbital periods, respectively.

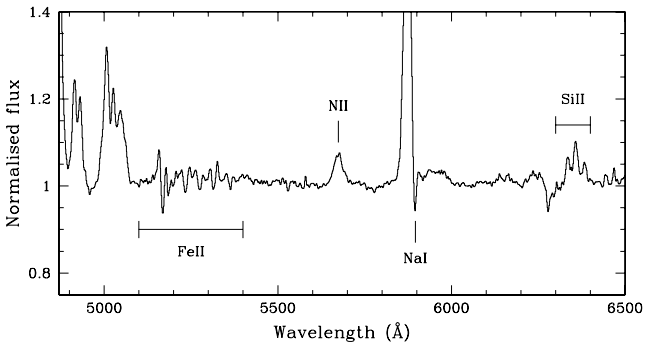

Figure 7. Orbitally averaged spectrum of HS 0220+0603. Note the unusual N II λ5680 emission line.

not the actual systemic velocity and radial velocity amplitude of the white dwarf (K_1). The Hα line in HS 0129+2933, HS 0220+0603 and HS 0455+8315 is delayed with respect to the motion of the white dwarf by $\varphi_0 \sim 0.2$. The He II λ4686 radial velocity curves of HS 0220+0603 and HS 0455+8315 show the same phase offset. This phase lag indicates that the main emission site is at an angle (∼72°) to the line of centres between the centre of mass of the binary and the white dwarf. The radial velocity curves are not sinusoidal in shape, showing significant distortion mainly at phases 0 (mid-eclipse) and 0.5. The spikes at $\varphi \sim 0$ are due to a rotational disturbance, caused by the fact that the secondary first occults the disc material approaching us and then the receding material. This translates into a red velocity spike before mid-eclipse and a blue spike after it.

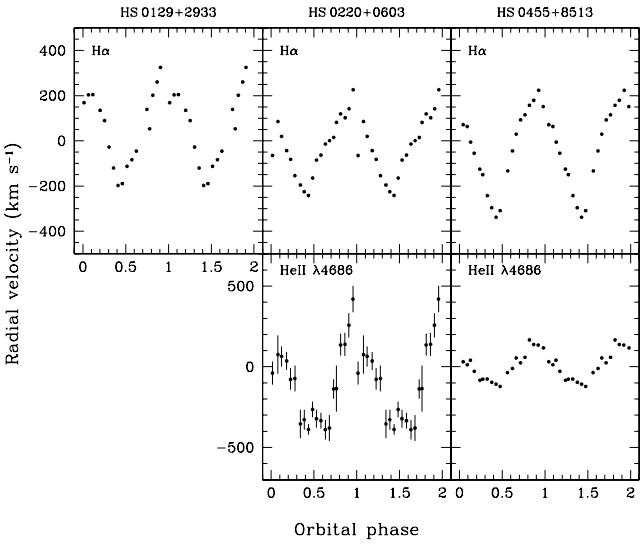

Figure 8. Radial velocity curves of the deeply eclipsing systems HS 0129+2933, HS 0220+0603 and HS 0455+8315 folded on their respective orbital periods after averaging the data into 20 phase bins. The Hα velocities are delayed by ∼0.1–0.2 orbital cycle with respect to the photometric ephemerides. The same is observed for the He II λ4686 lines in HS 0220+0603 and HS 0455+8315. The orbital cycle has been plotted twice.

Table 5. Radial velocity curve fitting parameters.

Line	γ (km s^{-1})	K (km s^{-1})	φ_0
HS 0129+2933			
Hα	69 ± 1	282 ± 1	0.240 ± 0.001
HS 0220+0603			
Hα	−37.0 ± 0.7	186 ± 1	0.170 ± 0.001
He II λ4686	−88 ± 16	295 ± 22	0.24 ± 0.01
HS 0455+8513			
Hα	−27 ± 1	238 ± 1	0.155 ± 0.001
He II λ4686	5 ± 1	125 ± 7	0.14 ± 0.01

4.3 The orbital period of HS 1813+6122

Of the five new CVs, HS 1813+6122 is the only one not showing eclipses, but the photometry suggests a possible orbital period of 3.54 h (Section 3.3). In an attempt to confirm this value we performed a period analysis on the Hα and Hβ radial velocities. The velocities were derived by using the double Gaussian method of Schneider & Young (1980) (which gave better results than the single Gaussian technique), adopting a Gaussian FWHM of 200 km s^{-1} and a separation of 1600 km s^{-1}. The 2002 September 1 and 2003 May INT data were obtained under poor observing conditions and were therefore excluded from the analysis. In Fig. 9, we show the resulting analysis-of-variance periodogram computed from the combined Hα and Hβ radial velocity curves. The periodogram shows its strongest peak at a period of 3.53 h, which confirms the value given by the photometric data as well as the presence of a negative superhump in the light curve of HS 1813+6122. A sine fit to the longest spectroscopic run (2003 June 29) with the period fixed at the above value yielded a tentative zero-phase time of T_0(HJD) = 245 2819.597(2). A preliminary trailed spectrum revealed the characteristic SW Sex

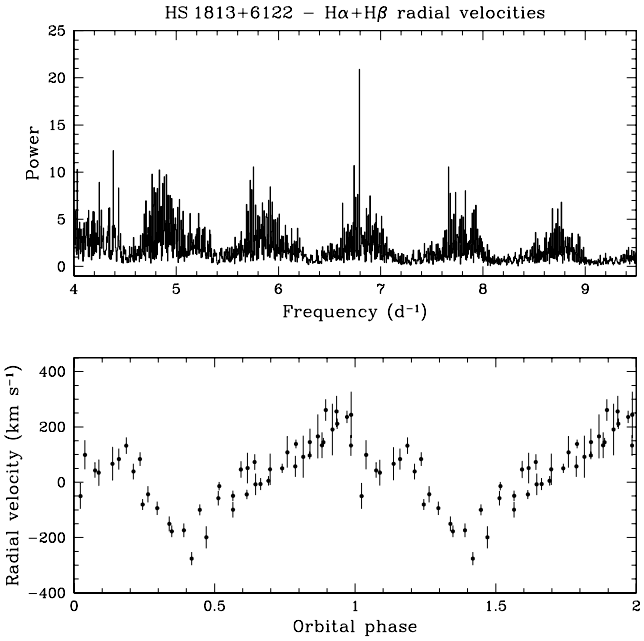

Figure 9. Top panel: Scargle periodogram of the Hα+Hβ radial velocity curves of HS 1813+6122. Bottom panel: phase-folded radial velocity curve (no phase binning applied). See the text for details on the adopted T_0. A full cycle has been repeated.

high-velocity S-wave reaching its maximum blue velocity at relative phase ∼0.3 (the phases are defined by using the above T_0). By analogy with the eclipsing systems presented in this paper (Section 4.4), and with the eclipsing SW Sex stars in general (see e.g. Hellier 1996; Hoard & Szkody 1997; Hellier 2000; Rodríguez-Gil et al. 2001), this is expected to happen at absolute phase $\varphi \sim 0.5$. Therefore, the Balmer radial velocities of HS 1813+6122 are delayed by $\varphi_0 \sim 0.2$ with respect to the white dwarf motion, a defining characteristic of the SW Sex stars. Correcting for this we get a new time of zero phase of T_0(HJD) = 245 2819.568(2). Fig. 9 shows the combined Hα and Hβ velocities folded on the orbital period with the new phase definition.

4.4 Trailed spectra

Trailed spectrograms of several emission lines of HS 0129+2933, HS 0220+0603 and HS 0455+8315 were constructed after rebinning the spectra on to an uniform velocity scale centred on the rest wavelength of each line. They are shown in Fig. 10. The Hα and Hβ line emission is dominated by a high-velocity emission component which follows neither the phasing of the primary nor that of the secondary. These S-waves reach their bluest velocity at $\varphi \sim 0.5$ in the three eclipsing systems and have a velocity amplitude of $\gtrsim$600 km s^{-1}. Weaker emission can also be seen underneath the dominant S-wave, possibly originating in the accretion disc. An absorption component is observed moving across the lines from red to blue, reaching maximum strength also at $\varphi \sim 0.5$.

The He I lines also display this high-velocity S-wave with the same phasing as the Balmer lines, as well as the absorption component. The He I λ4472 line in HS 0220+0603 shows it for approximately three quarters of an orbit, going well below the continuum.

Only HS 0220+0603 and HS 0455+8315 have a He II λ4686 line strong enough to produce a clear trailed spectrogram. While in the former the emission seems to be entirely dominated by the high-velocity component, two components are observed in the latter: a low-velocity one (the strongest), and a weaker component which is probably the same S-wave we observe in the Balmer and He I lines. No significant absorption is detected in He II λ4686.

In Fig. 11, we present the Hα trailed spectrum of HS 1813+6122 after averaging the individual spectra into 20 orbital phase bins. The line shows a high-velocity S-wave with maximum blue velocity at ~ -2000 km s^{-1}.

4.5 The FUV spectrum of HS 0455+8315

The UV spectrum of HS 0455+8315 (obtained at $\varphi \simeq 0.75$) displays very strong emission lines of He, C, N, O and Si, with line flux ratios compatible with those observed in the majority of CVs (Mauche, Lee & Kallman 1997), indicating normal chemical abundances of the donor star (see Fig. 12). The slope of the FUV continuum is nearly flat as observed in a number of deeply eclipsing SW Sex stars (e.g. DW UMa, Szkody 1987; Knigge et al. 2004; PX And, Thorstensen et al. 1991b; BH Lyn, Hoard & Szkody 1997). It has been argued that a relatively cold structure shields the inner disc and the white dwarf from view in high-inclination SW Sex stars during the high state, specifically supported by the FUV detection of the hot white dwarf in DW UMa during a low state (Knigge et al. 2000; Araujo-Betancor et al. 2003).

5 SW Sex MEMBERSHIP

The five new CVs presented in this paper have very much in common. In their average spectra the Balmer and He I lines display both single- or double-peaked profiles. The double-peaked profiles are likely a consequence of phase-dependent absorption components as the trailed spectra show. The lines are also characterized by highly asymmetric profiles with enhanced wings. The trailed spectra reveal the presence of a high-velocity emission S-wave in all the systems with extended wings reaching a maximum velocity between $\sim \pm 2000$ km s^{-1} (HS 1813+6122) and $\sim \pm 1000$ km s^{-1} in the eclipsing systems. The tendency of non-eclipsing SW Sex stars to show broader S-waves may be evidence of emitting material with a vertical velocity gradient such as a mass outflow.

The radial velocity curves also show a distinctive SW Sex feature. They are delayed with respect to the motion of the white dwarf, so that the red-to-blue crossing takes place at $\varphi \sim 0.2$ instead of $\varphi = 0$. On the other hand, the eclipsing systems also display a discontinuity around mid-eclipse, probably a rotational disturbance, which indicates that part of the line emission comes from the accretion disc.

All the features described above are defining characteristics of the SW Sex stars (see Thorstensen et al. 1991b; Rodríguez-Gil, Schmidtobreick & Gänsicke 2007). Even though each system exhibits its own peculiarities (e.g. unusual spectral lines in HS 0220+0603 and strong He II λ4686 emission in HS 0455+8315), they all share the characteristic SW Sex behaviour. We therefore classify them all as new SW Sex stars.

6 THE SW Sex STARS IN THE CONTEXT OF CATACLYSMIC VARIABLE EVOLUTION

6.1 How are the SW Sex stars discovered as CVs?

CVs are found by a number of means. Many of them display abrupt brightenings as a result of a dwarf nova eruption or a nova explosion.

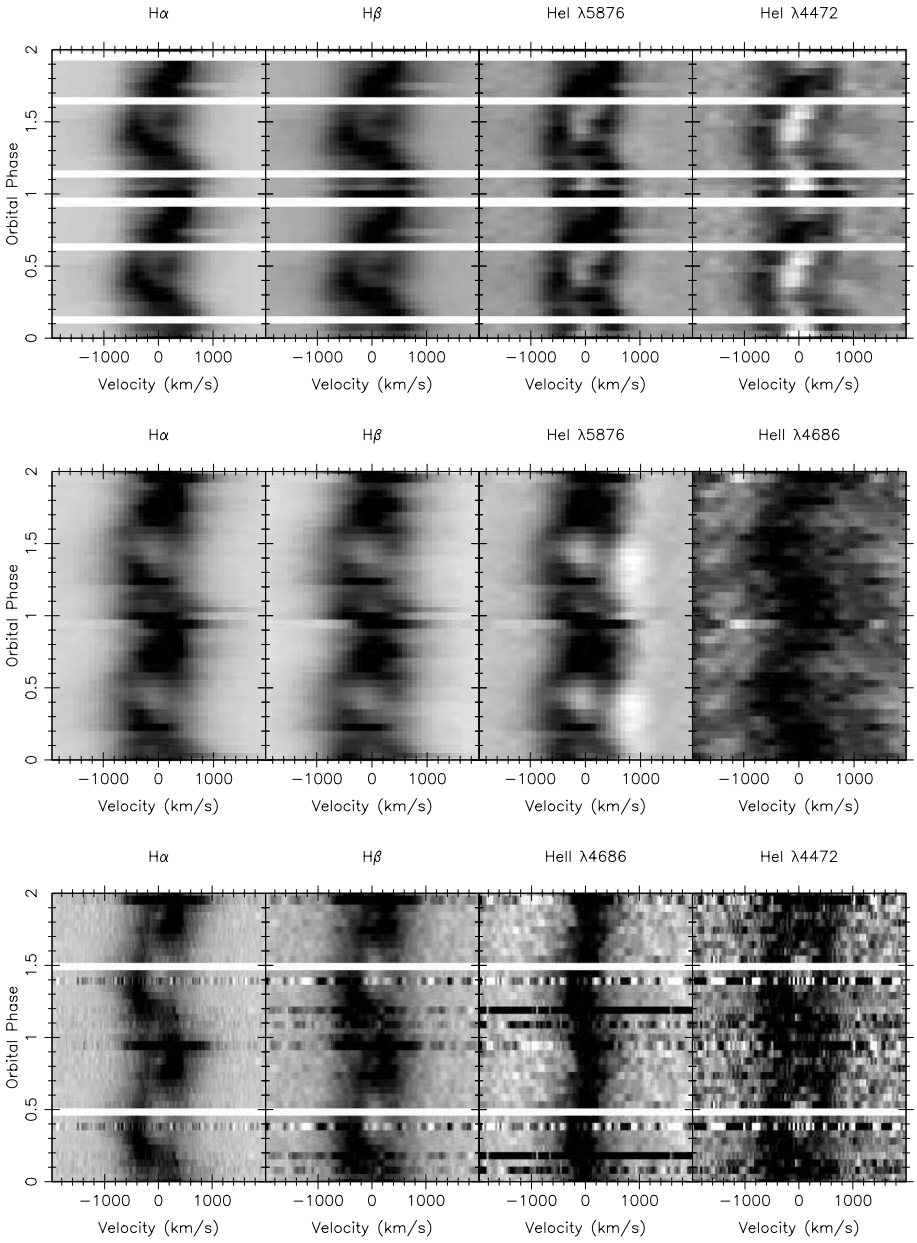

Figure 10. Trailed spectra of (from top to bottom panel) HS 0129+2933, HS 0220+0603 and HS 0455+8513. The individual spectra were averaged into 20 phase bins. Black represents emission. Unsampled phase bins are indicated by a blank spectrum. A full orbital cycle has been repeated for continuity.

They also show a rich variety of photometric variations like eclipses, orbital modulations, rapid oscillations, ellipsoidal modulations, etc. Others have been discovered by their blue colour, the emission of X-rays, or the presence of strong emission lines in their optical spectra.

The total number of definite members of the SW Sex class so far known amounts to 35, out of which a remarkable number of 18 (51 per cent) have been found in UV-excess surveys (i.e. blue colour). This is not surprising, as the optical spectra of the SW Sex stars in the high state are characterized by a very blue continuum. On the other hand, 11 SW Sex stars (31 per cent) have been identified as CVs from their emission-line spectra, five of which were discovered in the HQS. Only four and two SW Sex stars have been found because of their brightness variability (including three novae) and X-ray emission, respectively.

Any sort of CV search has its own selection effects, and the classification of a CV as an SW Sex star is no exception. In fact, the deep eclipses that many of the SW Sex stars show initially made the sample clearly biased towards high-inclination systems. This led many authors to link the SW Sex phenomenon to a mere inclination effect. At the last count, 13 out of a total of 35 SW Sex stars (37 per cent) do not display eclipses and are *bona fide* members of the class. Although an inclination effect may certainly be important (see the case of HL Aqr in Rodríguez-Gil, Schmidtobreick & Gänsicke 2007), the increasing number of non-eclipsing systems poses serious difficulties to any model resting solely on a high orbital inclination.

In the following section, we discuss on the impact of SW Sex stars in the (spectroscopic) HQS sample, which is unaffected by the high-inclination selection effect.

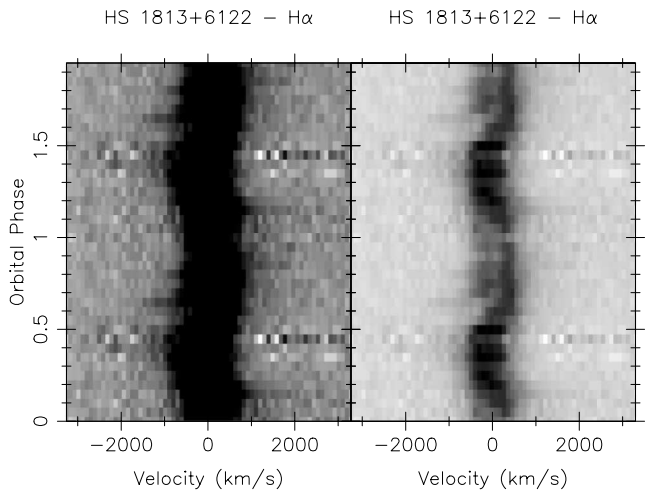

Figure 11. Hα trailed spectra of HS 1813+6122. Black represents emission. The grey-scale has been adjusted to enhance the high-velocity S-wave (left-hand panel) and the line core (right-hand panel). A whole cycle has been repeated.

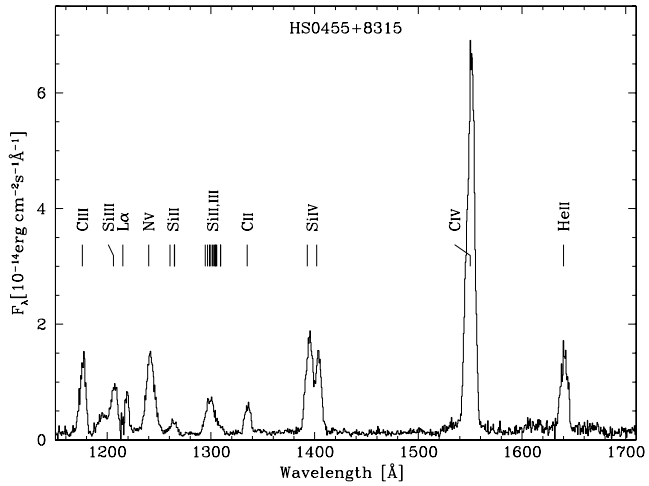

Figure 12. *HST*/STIS FUV spectrum of HS 0455+8315.

6.2 The role of the SW Sex stars in the big family of nova-like CVs

In Table 6, we list the 35 known SW Sex stars along with their orbital periods. Before doing any statistics we want to stress the fact that Table 6 does not intend to present a definitive census of the SW Sex stars. This is because their defining characteristics are continuously evolving as we dig deeper into the understanding of this class of CVs. For comparison (and probably completeness) we also point the reader to Don Hoard's *Big List of SW Sex stars*.[3]

Table 6 shows that a significant 37 per cent of the family do not show eclipses, confirming that the high-inclination requirement is merely a selection effect. The orbital period distribution of the known sample of SW Sex stars is presented in the left-hand panel of Fig. 13. The combined distributions for non-SW Sex nova-likes and nova remnants are also plotted for comparison. The nova-likes and novae were selected from the Ritter (Ritter & Kolb 2003), CVcat (Kube et al. 2003), and Downes (Downes et al. 2005) catalogues. Only systems with a robust orbital period determination are included.

These orbital period distributions reveal important features. About 40 per cent (35 out of 93) of the whole nova-like/classical nova population (which is preferentially found above the period gap; only 12 are below it) are indeed SW Sex stars. Even more remarkable is the fact that the SW Sex stars represent almost *half* (26 out of 53) the CVs in the narrow 3–4.5 h orbital period range. Above 4.5 h things radically change and only 14 per cent (four out of 28) of the nova-like/nova population are known to be SW Sex stars. The impact of SW Sex stars in the gap is also striking, as 55 per cent of all the nova-like/nova gap inhabitants are members of the class.

The non-SW Sex nova-like/nova $P_{\rm orb}$ distribution also shows a significant fraction of systems in the 3–4.5 h interval. This nicely

[3] http://spider.ipac.caltech.edu/staff/hoard/biglist.html.

Table 6. The SW Sex stars.

Object	$P_{\rm orb}$ (h)	Eclipses	References
V348 Pup	2.44	Yes	1
V795 Her	2.60	No	2
RX J1643.7+3402	2.89	No	3
V442 Oph	2.98	No	4
AH Men	3.05	No	5
HS 0728+6738	3.21	Yes	6
HS 0805+3822	3.21	Grazing	7, this paper
SW Sex	3.24	Yes	8
HL Aqr	3.25	No	5
DW UMa	3.28	Yes	8
SDSS J132723.39+652854.2	3.28	Yes	9
WX Ari	3.34	Grazing	10
HS 0129+2933	3.35	Yes	This paper
V1315 Aql	3.35	Yes	8
BO Cet	3.36	No	5
AH Pic	3.41	No	5
VZ Scl	3.47	Yes	11
LN UMa	3.47	No	5
RR Pic	3.48	Grazing	12
PX And	3.51	Yes	8
V533 Her	3.53	No	13
HS 1813+6122	3.54	No	This paper
HS 0455+8315	3.57	Yes	This paper
HS 0220+0603	3.58	Yes	This paper
HS 0357+0614	3.59	No	14
V380 Oph	3.70	No	5
BH Lyn	3.74	Yes	15
UU Aqr	3.93	Yes	16
LX Ser	3.95	Yes	17
V1776 Cyg	3.95	Yes	18
LS Peg	4.19	No	19
V347 Pup	5.57	Yes	20
RW Tri	5.57	Yes	21
V363 Aur	7.71	Yes	22
BT Mon	8.01	Yes	23

References. 1 Rodríguez-Gil et al. (2001); 2 Casares et al. (1996); 3 Mickaelian et al. (2002); 4 Hoard et al. (2000); 5 Rodríguez-Gil, Schmidtobreick & Gänsicke (2007); 6 Rodríguez-Gil et al. (2004); 7 Szkody et al. (2003); 8 Thorstensen et al. (1991b); 9 Wolfe et al. (2003); 10 Beuermann et al. (1992); 11 Moustakas & Schlegel (1999); 12 Schmidtobreick, Tappert & Saviane (2003); 13 Rodríguez-Gil & Martínez-Pais (2002); 14 Szkody et al. (2001); 15 Thorstensen et al. (1991a); 16 Hoard et al. (1998); 17 Young, Schneider & Shectman (1981); 18 Garnavich et al. (1990); 19 Taylor et al. (1999); 20 Thoroughgood et al. (2005); 21 Groot, Rutten & van Paradijs (2004); 22 Thoroughgood et al. (2004); 23 Smith et al. (1998)

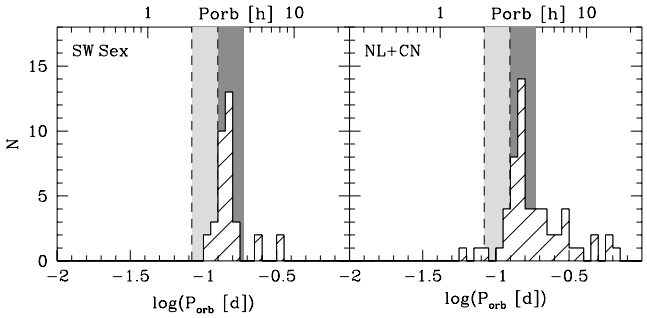

Figure 13. Period distributions of confirmed SW Sex stars (left-hand panel) and nova-like variables and classical novae that are not known to exhibit SW Sex behaviour. The orbital period gap and the 3–4 h orbital period range are indicated in light and dark grey, respectively.

depicts the tendency of nova-likes to accumulate in the 3–4.5 h period range. Therefore, it is very likely that more SW Sex stars are still to be found. In fact, time-resolved spectroscopic studies like the one reported in Rodríguez-Gil, Schmidtobreick & Gänsicke (2007) are revealing the SW Sex nature of many previously poorly studied nova-likes in this range. If the rate of detection and identification of SW Sex systems remains high, the dominance of this class at the upper edge of the gap will eventually become even more pronounced.

It is possible, however, that these numbers are the result of a selection effect as the majority of SW Sex stars are bright, making them easily accessible to observations. Therefore, one can argue that a proper characterization of the whole population of CVs above the gap needs to be made before addressing any conclusion. However, the fact that the majority of SW Sex stars have orbital periods between 3 and 4.5 h is a well established fact.

6.2.1 The impact of SW Sex stars on the HQS CV sample

During the course of our spectroscopic search we have discovered 53 new CVs in the area/magnitude range covered by the HQS ($\simeq$13 600 deg^2/17.5 $\lesssim B \lesssim$ 18.5; see Hagen et al. 1995). So far, we have determined the orbital period for 43 of them in a huge observational effort. Our preliminary results support the SW Sex excess within the 3–4.5 h range. Remarkably, 54 per cent (seven out of 13) of all the newly discovered HQS nova-likes are indeed SW Sex stars, which is in agreement with the distribution discussed above. This gives further strength to the significancy of the observed (and still unexplained) pile-up of SW Sex stars in the 3–4.5 h region.

6.3 CV evolution and the SW Sex stars

This accumulation of systems just above the period gap seriously challenges our current understanding of CV evolution. The SW Sex stars are intrinsically very luminous, as the brightness of systems like DW UMa indicates. DW UMa is an SW Sex star likely located at a distance between $\sim$590 and 930 pc (Araujo-Betancor et al. 2003) that has an average magnitude of $V \sim 14.5$, even though it is viewed at an orbital inclination of $\sim$82°. Therefore, in order to show such high luminosities, either the SW Sex stars have an average mass-transfer rate well above that of their CV cousins, or another source of luminosity exists. Neither the Rappaport, Joss & Verbunt (1983) nor the (empirical) Sills, Pinsonneault & Terndrup (2000) angular momentum loss prescriptions account for a largely enhanced mass-transfer rate ($\dot{M}$) in the period interval where most of the SW Sex stars reside. In this regard, nuclear burning has been suggested as an extra luminosity source (Honeycutt 2001), but the necessary conditions for the burning to occur can only be found in the base of a magnetic accretion funnel, suggesting a magnetic nature (Honeycutt & Kafka 2004). Temporary cessation of nuclear burning would, in principle, explain the VY Scl low states that many SW Sex and other nova-likes undergo. If this is true, the majority of CVs above the period gap have to be magnetic, in stark contrast with a non-magnetic majority below the gap. However, the fact that some dwarf novae (like HT Cas and RX And) also show low states (e.g. Robertson & Honeycutt 1996; Schreiber, Gänsicke & Mattei 2002) argues against this possibility, suggesting that the VY Scl states are likely the product of a decrease in the mass-transfer rate from the donor star caused by star-spots, as already proposed by Livio & Pringle (1994). The observational results of Honeycutt & Kafka (2004) appear to support this hypothesis (see also e.g. Howell et al. 2000).

All of the above arguments point to accretion at a very high $\dot{M}$ as the most likely cause for the high luminosity observed in the SW Sex stars. One possibility could be enhanced mass transfer due to irradiation of the inner face of the secondary star by a very hot white dwarf. In fact, a number of nova-like CVs in the $\sim$3–4 h orbital period range (including the SW Sex star DW UMa) have been observed to harbour the hottest white dwarfs found in any CV (see Araujo-Betancor et al. 2005), with effective temperatures peaking at $\sim$50 000 K. These high temperatures are most likely the result of accretion heating, as CVs are thought to spend on average $\sim$2 Gyr as detached binary systems (Schreiber & Gänsicke 2003), enough time for the white dwarfs to cool down to $\lesssim$ 8000 K. Hence, the high effective temperatures measured in the 3−4 h range is a measure of a very high secular mass-accretion rate of $\sim 5 \times 10^{-9}\,\mathrm{M}_\odot\,\mathrm{yr}^{-1}$ (Townsley & Bildsten 2003), higher than that predicted by angular momentum loss due to magnetic braking. Irradiation of the donor star has been observed in the non-eclipsing SW Sex stars HL Aqr, BO Cet and AH Pic (Rodríguez-Gil, Schmidtobreick & Gänsicke 2007), which supports the above hypothesis. Alas, the question of why the SW Sex stars have the highest mass-transfer rates is still lacking a satisfactory explanation in the context of the current CV evolution theory.

6.4 A rich phenomenology to explore

It is becoming apparent that the SW Sex phenomenon is not restricted to the (mainly) spectroscopic properties initially introduced by Thorstensen et al. (1991b). These maverick CVs are now known to show a much more intricate behaviour. Therefore, only a comprehensive study of this rich phenomenology will definitely lead to a full understanding of the SW Sex stars. In what follows we will review the range of common features exhibited by the SW Sex stars and which implications can be derived from them.

6.4.1 Superhumps

A significant one-third of the SW Sex stars are known to show apsidal (positive) or/and nodal (negative) superhumps, which are large-amplitude photometric waves modulated at a period slightly longer or slightly shorter than the orbital period, respectively. Positive superhumps are believed to be the effect of an eccentric disc which is forced to progradely precess by the tidal perturbation of the donor star (Whitehurst 1988). On the other hand, negative superhumps are likely linked to the retrograde precession of a warped accretion disc (Murray et al. 2002). Vertical changes in the structure of the disc

may be triggered by the torque exerted on the disc by the tilted, dipolar magnetic field of the secondary star. Apparently, positive and negative superhumps are independent and can either coexist or alternate with a time-scale of years.

The detection of superhumps in the SW Sex stars is of great importance as they exhibit the largest superhump period excesses. Therefore, they are fundamental in calibrating the period excess–mass ratio relationship for CVs (see Patterson et al. 2005).

6.4.2 Variable eclipse depth

The continuum light curves of some eclipsing members of the class reveal that the eclipse depth varies with a time-scale of several days. So far this variability has only been studied in PX And (Stanishev et al. 2002; Boffin et al. 2003) and DW UMa (Bíró 2000; Stanishev et al. 2004, not to be confused with the changing eclipse depth in different brightness states). In PX And, Stanishev et al. (2002) identified this long periodicity with the precession period of the accretion disc, which may also be true for DW UMa. The actual mechanism is not yet understood, although the eclipses of a retrogradely precessing, warped disc may account for what is observed in PX And (Boffin et al. 2003).

6.4.3 Low states

Half of the nova-likes known to undergo VY Scl faint states are SW Sex stars. During these events the system brightness can drop by up to ∼4–5 mag and can remain that low for months. As the disc warping effect mentioned above, these low states may be controlled by the strong magnetic activity of the donor star, and are believed to be driven by a sudden drop in the accretion rate from the secondary star due to large star-spots located in the area around the inner Lagrangian point L_1 (Livio & Pringle 1994).

Interestingly, the disced VY Scl stars concentrate in the 3–4.5 h orbital period stripe as the SW Sex stars do. It would therefore not be a surprise to find that all nova-likes in that range are actually VY Scl stars and even SW Sex stars. Nevertheless, the presence of large star-spots around the L_1 point still have to be observationally confirmed. Using Roche tomography techniques, Watson, Dhillon & Shahbaz (2006) discovered a heavily spotted secondary star in AE Aqr ($P_{\rm orb} = 9.88$ h) with a spot distribution resembling that of other rapidly rotating, low-mass field stars. A stellar atmosphere plagued with spots has been also observed in the pre–CV V471 Tau ($P_{\rm orb} = 12.51$ h, Hussain et al. 2006). Unfortunately, the high spectral and time-resolution required to image the M dwarf donor in a CV with $P_{\rm orb} \simeq 3.5$ h at a distance of many hundred parsecs is currently beyond observational reach.

6.4.4 Quasi-periodic oscillations

On the grounds of short-term variability, the SW Sex stars are also characterized for exhibiting quasi-coherent modulations in their light curves. In a compilation of CVs displaying rapid oscillations, Warner (2004) lists nine (only two deeply eclipsing) SW Sex stars known to have quasi-periodic oscillations (QPOs) with a predominant time-scale of ∼1000–2000 s. For example, the non-eclipsing SW Sex stars V442 Oph and RX J1643.7+3402 show strong QPO signals dominating over other underlying higher-coherence oscillations (Patterson et al. 2002). These results are based on hundreds of hours of photometric data, whose power spectra showed rapid frequency changes in the main signals in less than a day. Similar rapid variability was also detected in the optical light curve of the SW Sex star HS 0728+6738 (Rodríguez-Gil et al. 2004), with a prominent signal (coherent for at least 20 cycles) at ∼600 s.

6.4.5 Emission-line flaring

In connection with the QPO activity, the fluxes and equivalent widths (EWs) of the emission lines of some SW Sex stars show modulations at the same time-scales (a phenomenon known as emission-line flaring): ∼1800 s in BT Mon (Smith, Dhillon & Marsh 1998), ∼2000 s in LS Peg (Rodríguez-Gil et al. 2001), ∼1400 s in V533 Her (Rodríguez-Gil & Martínez-Pais 2002), ∼1800 s in DW UMa (V. Dhillon, private communication), ∼2400 s in RX J1643.7+3402 (Martínez-Pais, de la Cruz Rodríguez & Rodríguez-Gil 2007), and ∼1200 s in BO Cet (Rodríguez-Gil, Schmidtobreick & Gänsicke 2007). Remarkably, the radial velocities measured in the last two objects are also modulated at the flux/EW periodicities, which suggests that emission-line flaring has to do with the dynamics of the line-emitting source, and is not due to, for example, random fluctuations in the disc continuum emission. On the other hand, although DW UMa does exhibit emission-line flaring in the optical, such line variability was not detected in the FUV (Hoard et al. 2003). Since similar flaring in the optical is observed in the intermediate polar CVs (IPs; e.g. FO Aqr Marsh & Duck 1996) caused by the rotation of the magnetic white dwarf, all the described rapid variations seen in many SW Sex stars have been associated to the presence of magnetic white dwarfs (Rodríguez-Gil et al. 2001; Patterson et al. 2002). Nevertheless, the FUV data of DW UMa presented by Hoard et al. (2003) can also be explained with a stream overflow model, but do not necessary exclude a magnetic scenario either.

6.4.6 Variable circular polarization

Despite the fact that circular polarization is not commonly detected in the majority of IPs, it is a *sine qua non* condition for IP membership (see further requirements in Patterson 1994). The cyclotron radiation emitted by the accretion columns (built up by disc plasma forced by the magnetic field to supersonically fall on to the white dwarf surface) is known to be circularly polarized, thus the detection of a significant level of circular polarization is an unequivocal sign of magnetic accretion. This, and the possible magnetic nature of the QPO and line flaring activity prompted to the search for circular polarization in the SW Sex stars.

Rodríguez-Gil et al. (2001) found circular polarization modulated at 1776 s with a peak-to-peak amplitude of 0.3 per cent in LS Peg. Remarkably, the flaring observed in the Hβ high-velocity S-wave was modulated at 2010 s, which is just the synodic period between the polarization period and the orbital period. V795 Her also revealed variable circular polarization with a periodicity of 1170 s (or twice that) and showed an increasing polarization level with wavelength (Rodríguez-Gil et al. 2002) as is expected for cyclotron emission. In addition, RX J1643.7+3402 shows circular polarization modulated at 1163 s (Martínez-Pais et al. 2007).

The 1776-s period of LS Peg was confirmed by Baskill, Wheatley & Osborne (2005) who detected a coherent modulation at 1854 s in *ASCA* X-ray light curves. The coincidence of both periods indicates a common origin, with the X-ray period reported by Baskill et al. likely being a more accurate measurement of the white dwarf spin period.

Although polarimetric studies of many other SW Sex stars have to be done, the results obtained so far suggest that magnetic accretion

may play an important role in the SW Sex phenomenon. However, with the few such studies so far at hand it is not possible to address any conclusion regarding the impact of magnetism in the whole class.

Despite the broad implications in our understanding of accretion that the study of the SW Sex stars have, the quest for a successful, global explanation of the phenomenon has been unfruitful so far. This, in addition to the (yet unexplained) fact that the majority of SW Sex stars (and many nova-likes) largely populate the narrow orbital period stripe between 3 and 4.5 h, is seriously shaking the grounds on which CV evolution theory stands. Further study of these maverick systems will certainly provide fundamental clues to our understanding of CV evolution.

ACKNOWLEDGMENTS

In the memory of Emilios Harlaftis.

AA thanks the Royal Thai Government for a studentship. BTG was supported by a PPARC Advanced Fellowship. MAPT is supported by NASA LTSA grant NAG-5-10889. RS is supported by the Deutsches Zentrum für Luft und Raumfahrt (DLR) GmbH under contract No. FKZ 50 OR 0404. AS is supported by the Deutsche Forschungsgemeinschaft through grant Schw536/20-1. The HQS was supported by the Deutsche Forschungsgemeinschaft through grants Re 353/11 and Re 353/22.

This paper includes data taken at The McDonald Observatory of The University of Texas at Austin. It is also based in part on observations obtained at the German-Spanish Astronomical Center, Calar Alto, operated by the Max-Planck-Institut für Astronomie, Heidelberg, jointly with the Spanish National Commission for Astronomy, on observations made at the 1.2-m telescope, located at Kryoneri Korinthias, and owned by the National Observatory of Athens, Greece, on observations made with the Isaac Newton Telescope, which is operated on the island of La Palma by the Isaac Newton Group in the Spanish Observatorio del Roque de los Muchachos of the Instituto de Astrofísica de Canarias (IAC), on observations made with the 1.2-m telescope at the Fred Lawrence Whipple Observatory, a facility of the Smithsonian Institution, on observations made with the IAC80 telescope, operated on the island of Tenerife by the IAC in the Spanish Observatorio del Teide, on observations made with the OGS telescope, operated on the island of Tenerife by the European Space Agency, in the Spanish Observatorio del Teide of the IAC, and on observations made with the Nordic Optical Telescope, operated on the island of La Palma jointly by Denmark, Finland, Iceland, Norway, and Sweden, in the Spanish Observatorio del Roque de los Muchachos of the IAC, and on observations made with the NASA/ESA Hubble Space Telescope, obtained at the Space Telescope Science Institute, which is operated by the Association of Universities for Research in Astronomy, Inc., under NASA contract NAS 5-26555.

This publication makes use of data products from 2MASS, which is a joint project of the University of Massachusetts and the Infrared Processing and Analysis Center/California Institute of Technology, funded by the National Aeronautics and Space Administration and the National Science Foundation.

REFERENCES

Araujo-Betancor S., Gänsicke B. T., Long K. S., Beuermann K., de Martino D., Sion E. M., Szkody P., 2005, ApJ, 622, 589
Araujo-Betancor S. et al., 2003, ApJ, 583, 437
Aungwerojwit A. et al., 2005, A&A, 443, 995
Baskill D. S., Wheatley P. J., Osborne J. P., 2005, MNRAS, 357, 626
Bertin E., Arnouts S., 1996, A&AS, 117, 393
Beuermann K., Thorstensen J. R., Schwope A. D., Ringwald F. A., Sahin H., 1992, A&A, 256, 442
Bíró I. B., 2000, A&A, 364, 573
Boffin H. M. J., Stanishev V., Kraicheva Z., Genkov V., 2003, in Sterken C., ed., ASP Conf. Ser. Vol. 292, Interplay of Periodic, Cyclic and Stochastic Variability in Selected Areas of the H-R Diagram. Astron. Soc. Pac., San Francisco, p. 297
Bonnet-Bidaud J. M., Mouchet M., 1987, A&A, 188, 89
Casares J., Martínez-Pais I. G., Marsh T. R., Charles P. A., Lázaro C., 1996, MNRAS, 278, 219
Dhillon V. S., Jones D. H. P., Marsh T. R., Smith R. C., 1992, MNRAS, 258, 225
Downes R. A., Webbink R. F., Shara M. M., Ritter H., Kolb U., Duerbeck H. W., 2005, VizieR Online Data Catalog, 5123
Gänsicke B. T., Araujo-Betancor S., Hagen H.-J., Harlaftis E. T., Kitsionas S., Dreizler S., Engels D., 2004, A&A, 418, 265
Gänsicke B. T. et al., 2003, ApJ, 594, 443
Gänsicke B. T., Hagen H. J., Engels D., 2002, in Gänsicke B. T., Beuermann K., Reinsch K., eds, ASP Conf. Ser. Vol. 261, The Physics of Cataclysmic Variables and Related Objects. Astron. Soc. Pac., San Francisco, p. 190
Garnavich P. M. et al., 1990, ApJ, 365, 696
Green R. F., Schmidt M., Liebert J., 1986, ApJS, 61, 305
Groot P. J., Rutten R. G. M., van Paradijs J., 2004, A&A, 417, 283
Hagen H. J., Groote D., Engels D., Reimers D., 1995, A&AS, 111, 195
Hameury J. M., Lasota J. P., 2002, A&A, 394, 231
Hellier C., 1996, ApJ, 471, 949
Hellier C., 2000, New Astron. Rev., 44, 131
Hellier C., Robinson E. L., 1994, ApJ, 431, L107
Hoard D. W., Szkody P., 1997, ApJ, 481, 433
Hoard D. W., Szkody P., Froning C. S., Long K. S., Knigge C., 2003, AJ, 126, 2473
Hoard D. W., Szkody P., Still M. D., Smith R. C., Buckley D. A. H., 1998, MNRAS, 294, 689
Hoard D. W., Thorstensen J. R., Szkody P., 2000, ApJ, 537, 936
Honeycutt R. K., 2001, PASP, 113, 473
Honeycutt R. K., Kafka S., 2004, AJ, 128, 1279
Horne K., 1986, PASP, 98, 609
Horne K., 1999, in Hellier C., Mukai K., eds, ASP Conf. Ser. Vol. 157, Annapolis Workshop on Magnetic Cataclysmic Variables. Astron. Soc. Pac., San Francisco, p. 349
Howell S. B., Ciardi D. R., Dhillon V. S., Skidmore W., 2000, ApJ, 530, 904
Hussain G. A. J., Allende Prieto C., Saar S. H., Still M., 2006, MNRAS, 367, 1699
Jameson R. F., King A. R., Sherrington M. R., 1980, MNRAS, 191, 559
Knigge C., Araujo-Betancor S., Gänsicke B. T., Long K. S., Szkody P., Hoard D. W., Hynes R. I., Dhillon V. S., 2004, ApJ, 615, L129
Knigge C., Long K. S., Hoard D. W., Szkody P., Dhillon V. S., 2000, ApJ, 539, L49
Kube J., Gänsicke B. T., Euchner F., Hoffmann B., 2003, A&A, 404, 1159
Livio M., Pringle J. E., 1994, ApJ, 427, 956
Marsh T. R., Duck S. R., 1996, New Astron., 1, 97
Martínez-Pais I. G., de la Cruz Rodríguez J., Rodríguez-Gil P., 2007, MNRAS, submitted
Martínez-Pais I. G., Rodríguez-Gil P., Casares J., 1999, MNRAS, 305, 661
Mauche C. W., Lee Y. P., Kallman T. R., 1997, ApJ, 477, 832
Mickaelian A. M., Balayan S. K., Ilovaisky S. A., Chevalier C., Véron-Cetty M.-P., Véron P., 2002, A&A, 381, 894
Monet D. G. et al., 2003, AJ, 125, 984
Moustakas J., Schlegel E. M., 1999, BAAS, 31, 1421
Murray J. R., Chakrabarty D., Wynn G. A., Kramer L., 2002, MNRAS, 335, 247
Patterson J., 1994, PASP, 106, 209
Patterson J. et al., 2002, PASP, 114, 1364
Patterson J. et al., 2005, PASP, 117, 1204
Patterson J., Skillman D. R., 1994, PASP, 106, 1141

Penning W. R., Ferguson D. H., McGraw J. T., Liebert J., Green R. F., 1984, ApJ, 276, 233
Podsiadlowski P., Han Z., Rappaport S., 2003, MNRAS, 340, 1214
Rappaport S., Joss P. C., Verbunt F., 1983, ApJ, 275, 713
Ritter H., Kolb U., 2003, A&A, 404, 301
Robertson J. W., Honeycutt R. K., 1996, AJ, 112, 2248
Rodríguez-Gil P., 2005, in Hameury J.-M., Lasota J.-P., eds, ASP Conf. Ser. Vol. 330, The Astrophysics of Cataclysmic Variables and Related Objects. Astron. Soc. Pac., San Francisco, p. 335
Rodríguez-Gil P., Casares J., Dhillon V. S., Martínez-Pais I. G., 2000, A&A, 355, 181
Rodríguez-Gil P., Casares J., Martínez-Pais I. G., Hakala P., Steeghs D., 2001, ApJ, 548, L49
Rodríguez-Gil P., Casares J., Martínez-Pais I. G., Hakala P. J., 2002, in Gänsicke B. T., Beuermann K., Reinsch K., eds, ASP Conf. Ser. Vol. 261, The Physics of Cataclysmic Variables and Related Objects. Astron. Soc. Pac., San Francisco, p. 533
Rodríguez-Gil P., Gänsicke B. T., Barwig H., Hagen H.-J., Engels D., 2004, A&A, 424, 647
Rodríguez-Gil P. et al., 2005, A&A, 440, 701
Rodríguez-Gil P., Martínez-Pais I. G., 2002, MNRAS, 337, 209
Rodríguez-Gil P., Martínez-Pais I. G., Casares J., Villada M., van Zyl L., 2001, MNRAS, 328, 903
Rodríguez-Gil P., Schmidtobreick L., Gänsicke B. T., 2007, MNRAS, 374, 1359
Rolfe D. J., Haswell C. A., Patterson J., 2000, MNRAS, 317, 759
Romano G., 1978, Inf. Bull. Variable Stars, 1421, 1
Scargle J. D., 1982, ApJ, 263, 835
Schenker K., King A. R., Kolb U., Wynn G. A., Zhang Z., 2002, MNRAS, 337, 1105
Schmidtobreick L., Tappert C., Saviane I., 2003, MNRAS, 342, 145
Schneider D. P., Young P., 1980, ApJ, 238, 946
Schreiber M. R., Gänsicke B. T., 2003, A&A, 406, 305
Schreiber M. R., Gänsicke B. T., Mattei J. A., 2002, A&A, 384, L6
Schwarzenberg-Czerny A., 1996, ApJ, 460, L107
Shafter A. W., Hessman F. V., Zhang E.-H., 1988, ApJ, 327, 248
Sills A., Pinsonneault M. H., Terndrup D. M., 2000, ApJ, 534, 335
Smith D. A., Dhillon V. S., Marsh T. R., 1998, MNRAS, 296, 465
Stanishev V., Kraicheva Z., Boffin H. M. J., Genkov V., 2002, A&A, 394, 625
Stanishev V., Kraicheva Z., Boffin H. M. J., Genkov V., Papadaki C., Carpano S., 2004, A&A, 416, 1057
Szkody P., 1987, AJ, 94, 1055
Szkody P., Gänsicke B., Fried R. E., Heber U., Erb D. K., 2001, PASP, 113, 1215
Szkody P., Piché F., 1990, ApJ, 361, 235
Szkody P. et al., 2003, AJ, 126, 1499
Taylor C. J., Thorstensen J. R., Patterson J., 1999, PASP, 111, 184
Thoroughgood T. D. et al., 2005, MNRAS, 357, 881
Thoroughgood T. D., Dhillon V. S., Watson C. A., Buckley D. A. H., Steeghs D., Stevenson M. J., 2004, MNRAS, 353, 1135
Thorstensen J. R., Davis M. K., Ringwald F. A., 1991a, AJ, 102, 683
Thorstensen J. R., Ringwald F. A., Wade R. A., Schmidt G. D., Norsworthy J. E., 1991b, AJ, 102, 272
Thorstensen J. R., Fenton W. H., Patterson J., Kemp J., Halpern J., Baraffe I., 2002a, PASP, 114, 1117
Thorstensen J. R., Fenton W. H., Patterson J. O., Kemp J., Krajci T., Baraffe I., 2002b, ApJ, 567, L49
Townsley D. M., Bildsten L., 2003, ApJ, 596, L227
Warner B., 2004, PASP, 116, 115
Warren S. R., Shafter A. W., Reed J. K., 2006, PASP, 118, 1373
Watson C. A., Dhillon V. S., Shahbaz T., 2006, MNRAS, 368, 637
Whitehurst R., 1988, MNRAS, 232, 35
Williams R. E., 1989, AJ, 97, 1752
Wolfe M. A., Szkody P., Fraser O. J., Homer L., Skinner S., Silvestri N. M., 2003, PASP, 115, 1118
Young P., Schneider D. P., Shectman S. A., 1981, ApJ, 244, 259

This paper has been typeset from a TEX/LATEX file prepared by the author.